

Inhibition of oxidative metabolism leads to p53 genetic inactivation and transformation in neural stem cells

Bartesaghi, S; Graziano, V; Galavotti, S; Henriquez, NV; Betts, J; Saxena, J; Minieria, V; Deli, A; Karlsson, A; Miguel Martins, L; Capasso, M; Nicotera, P; Brandner, S; De Laurenzi, V; Salomoni, P

For additional information about this publication click this link.

<http://qmro.qmul.ac.uk/jspui/handle/123456789/6879>

Information about this research object was correct at the time of download; we occasionally make corrections to records, please therefore check the published record when citing. For more information contact scholarlycommunications@qmul.ac.uk

Inhibition of oxidative metabolism leads to p53 genetic inactivation and transformation in neural stem cells

Stefano Bartesaghi¹, Vincenzo Graziano^{1,2*}, Sara Galavotti^{1*}, Nick Henriquez^{3*}, Joanne Betts-Henderson¹, Jayeta Saxena¹, A Deli¹, Anna Karlsson⁴, L. Miguel Martins⁵, Melania Capasso⁶, Pierluigi Nicotera⁷, Sebastian Brandner³, Vincenzo De Laurenzi², and Paolo Salomoni¹

¹Samantha Dickson Brain Cancer Unit, University College London, United Kingdom; ²Department of Experimental and Clinical Sciences, Aging Research Center (Ce.S.I.), University G. d'Annunzio, Chieti-Pescara, Italy; ³Institute of Neurology, University College London, United Kingdom; ⁴Karolinska Institute, Stockholm, Sweden; ⁵MRC Toxicology Unit, Leicester, United Kingdom; ⁶Barts Cancer Institute, Queen Mary University, London, United Kingdom; ⁷DZNE, Bonn, Germany. *These authors contributed equally to this work

Submitted to Proceedings of the National Academy of Sciences of the United States of America

Alterations of mitochondrial metabolism and genomic instability have been implicated in tumorigenesis in multiple tissues. High-grade glioma (HGG), one of the most lethal human neoplasms, displays genetic modifications of Krebs cycle components as well as electron transport chain (ETC) alterations. Furthermore, the p53 tumor suppressor, which has emerged as a key regulator of mitochondrial respiration at the expense of glycolysis, is genetically inactivated in a large proportion of HGG cases. Therefore, it is becoming evident that genetic modifications can affect cell metabolism in HGG, however it is currently unclear whether mitochondrial metabolism alterations could vice versa promote genomic instability as a mechanism for neoplastic transformation. Here, we show that in neural progenitor/stem cells (NPCs), which can act as HGG cell of origin, inhibition of mitochondrial metabolism leads to p53 genetic inactivation. Impairment of respiration via inhibition of complex I or decreased mitochondrial DNA copy number leads to p53 genetic loss and a glycolytic switch. p53 genetic inactivation in ETC-impaired neural stem cells is caused by increased ROS and associated oxidative DNA damage. ETC-impaired cells display a marked growth advantage in the presence or absence of oncogenic RAS, and form undifferentiated tumors when transplanted into the mouse brain. Finally, p53 mutations correlated with alterations in ETC subunit composition and activity in primary glioma-initiating neural stem cells. Together, these findings provide novel insights into the relationship between mitochondria, genomic stability and tumor suppressive control, with implications for our understanding of brain cancer pathogenesis.

p53 | metabolism | glioma

Introduction

Alterations of mitochondrial metabolism are found in several cancers (1). This can occur through inactivation of components of the tricarboxylic acid (TCA) cycle and electron transport chain (ETC) (1-5). In particular, a substantial proportion of high-grade gliomas (HGG), display mutations in the isocitrate dehydrogenase TCA enzymes *IDH1* and *IDH2*. Notably, gliomas also present mutations in mitochondrial DNA (mtDNA) and alterations of the ETC, but whether these are early or late events in cancer pathogenesis remains to be determined (6-14). Finally p53, which has emerged as an important regulator of mitochondrial metabolism and cellular redox control (15-17), is often found mutated or functionally inactivated in HGG. Its inactivation in neural progenitor/stem cells (NPCs), which act as HGG cells of origin, contributes to gliomagenesis (18-22). In particular, deletion of a significant portion of the p53 DNA binding domain induces the accumulation of cooperative oncogenic events, thus leading to HGG (21). However, it remains to be determined whether p53 metabolic functions contribute to suppression of neoplastic transformation in the nervous system. Although these studies suggest an involvement of altered mitochondria metabolism in brain tumorigenesis, direct evidence of

its role as a cancer driver or contributing factor is missing. More generally, the role of mitochondrial dysfunction in regulation of tumor suppressive control remains only partially investigated.

Here, we studied the effect of oxidative metabolism inhibition in normal NPCs. Our findings show that inhibition of respiration via knockdown of the complex I subunit NDUFA10 or by reducing mtDNA copy number results in p53 genetic loss, via a mechanism involving generation of reactive oxygen species (ROS) and ROS-mediated oxidative damage. In turn, this causes a glycolytic switch, a marked growth advantage and tumor formation upon transplantation in the mouse brain. Overall, this study reveals that in NPCs the relationship between p53 and mitochondrial metabolism is bidirectional, with p53 being activator of mitochondrial metabolism as well as target for genetic inactivation upon inhibition of respiratory chain activity.

Results

We studied the effect of oxidative metabolism inhibition in NPCs derived from the sub-ventricular zone (SVZ), one of the two main postnatal neurogenic niches involved in brain tumorigenesis (20, 23). To this end, we inhibited the ETC by knocking down the ETC complex I component NADH dehydrogenase (ubiquinone) 1 alpha sub-complex, 10 of complex I (NDUFA10) (Suppl. Fig. 1A). shRNA-mediated NDUFA10 knockdown resulted in decreased oxygen consumption rate (OCR) both at steady state

Significance

Brain cancer is one of the deadliest human tumors and is characterized by several genetic changes leading to impairment of tumor suppressive pathways and oncogene activation. These genetic alterations promote subsequent molecular changes, including modifications of cellular metabolism, which are believed to contribute to cancer pathogenesis. Conversely, the role of metabolic changes in regulation of genomic stability in brain cancer has not been investigated. Our work shows that alterations of mitochondrial metabolism promote genetic loss of the p53 tumor suppressor and transformation via a mechanism involving reactive oxygen species. Overall, our findings suggest a causative link between metabolic alterations and loss of tumor suppressive control in the central nervous system, with implications for our understanding of brain cancer pathogenesis.

Reserved for Publication Footnotes

137
138
139
140
141
142
143
144
145
146
147
148
149
150
151
152
153
154
155
156
157
158
159
160
161
162
163
164
165
166
167
168
169
170
171
172
173
174
175
176
177
178
179
180
181
182
183
184
185
186
187
188
189
190
191
192
193
194
195
196
197
198
199
200
201
202
203
204

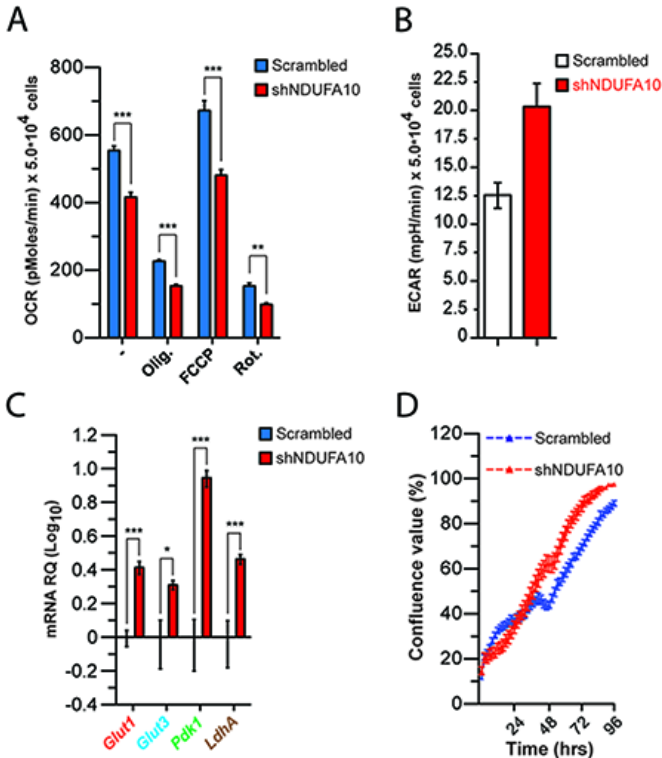


Fig. 1. Silencing of a complex I component results in metabolic shift and growth advantage in NPCs(A) OCR in shNDUFA10 NPCs under basal conditions, following addition of oligomycin (0.1 $\mu\text{g ml}^{-1}$), FCCP (0.4 μM), or rotenone (0.2 μM) (Data are represented as mean \pm SEM for n=3; **p<0.01, ***p<0.001); (B) ECAR in scramble and shNDUFA10 transfected NPCs. Lactate production was measured under basal conditions or after oligomycin treatment; (C) QPCR expression analysis of genes involved in glucose uptake and metabolism in scrambled and shNDUFA10 NPCs. Results are normalized to β -actin expression levels (n=3 *p<0.05, **p<0.01, ***p<0.001); (D) Cell growth of scrambled and shNDUFA10 transduced NPCs, as assessed by INCUCYTE™ Live-Cell Imaging System.

and upon treatment with the complex I inhibitor rotenone and complex V inhibitor oligomycin (Fig. 1A). Maximal respiration was also reduced in shNDUFA10 cells (Fig. 1A). Diminished ETC activity was associated with increased extracellular acidification rate (ECAR) and lactate levels (Fig. 1B and Suppl. Fig. 1B). In agreement with their glycolytic metabolism, shNDUFA10 cells displayed increased expression of genes involved in glucose uptake and metabolism *Glut1*, *Glut3*, *Pdk1* and *LdhA* (Fig. 1C). Finally, acquisition of glycolytic metabolism was associated with growth advantage (Fig. 1D). Thus, NPCs appears to activate glycolytic metabolism upon inhibition of ETC activity.

To determine whether these changes could occur also in another model of mitochondrial dysfunction, we used genetically modified NPCs, where oxidative phosphorylation is decreased due to loss of thymidine kinase 2 (TK2), a key component of the salvage pathway for nucleotide biosynthesis within mitochondria (24-26). K2 KO animals are ataxic and die by postnatal day 15 due to defects in multiple tissues (24-26). TK2 deficiency in postmitotic cells results in decreased mtDNA synthesis, in turn leading to diminished expression of mtDNA-encoded ETC components and impaired ETC (24-26). We isolated NPCs from the SVZ of WT and KO mice (preparation WT1 and KO1; Suppl. dataset 1). TK2 KO NPCs showed decreased mtDNA levels (Fig. 2A) and reduced expression of the mtDNA-encoded complex IV subunit I (C-IV-I) and the nuclear DNA-encoded C-INDUF8 (Fig. 2B). This in turn led to impaired mitochondrial oxidative capacity, as measured by detection of OCR (Fig. 2C). Defects in ETC func-

tion were accompanied by increased lactate and ATP levels (Fig. 2D, E). Notably, TK2 KO cells displayed increased expression of *Glut1*, *Pdk1* and *LdhA* (Fig. 2F). Short hairpin RNA (shRNA)-mediated knockdown (KD) of TK2 (Suppl. Fig. 1C) led to similar metabolic alterations (Suppl. Fig. 1D, E). Analysis of the TK2 KO metabolome revealed clear changes in glycolysis as well as sugar metabolism and Krebs cycle (Fig. 2G and Suppl. dataset 1). Overall, these data together with NDUFA10 knockdown experiments show that NPCs, unlike postmitotic neurons (25), are able to activate glycolysis upon inhibition of oxidative metabolism. These metabolic changes correlated with increased growth properties, as, when plated at clonal density in non-adherent conditions, KO NPCs formed larger neurospheres (Fig. 2H). Furthermore, in adherent conditions TK2 KO NPC cultures displayed an increased number of cells in S phase (Fig. 2I). This phenotype was not associated with changes in basal apoptosis (Suppl. Fig. 1F). When switched to differentiating conditions, TK2 KO cultures displayed an increased number of Nestin-positive undifferentiated cells and generated more TuJ1-positive neurons (Suppl. Fig. 2A-C). Finally when switched back to proliferation media, KO cells proliferated more readily and formed larger neurospheres (Suppl. Fig. 2D, E). These data indicate that ETC impairment leads to increased proliferation and altered differentiation properties in NPCs.

We next investigated the mechanisms underlying the metabolic switch to glycolysis in ETC-impaired NPCs. As these phenotypic changes are features of p53-deficient cells (17), we studied whether ETC-impaired cells displayed alterations of the p53 pathway. We observed a complete lack of full-length (FL) p53 expression and the presence of a shorter isoform (Δ p53) along with reduced p21 expression (Fig. 3A, Suppl. Fig. 3A and Table 1) in TK2 KO cells. In agreement with the loss of FL p53 and decreased p21 levels, KO cells failed to arrest upon ionizing irradiation (IR; Suppl. Fig. 3B). We sequenced p53 cDNA in search of potential mutations in its coding region and found a p53 truncation, which was caused by a 44-nucleotide deletion, which created a premature stop codon (Suppl. Fig. 3C). Interestingly, C-terminal p53 truncations have been described in HGG cells (27). We next analyzed two additional TK2 KO NPC preparations (Suppl. Table 1). KO2 cells carried a missense mutation in the p53 DNA binding domain (Suppl. Fig. 3C), which corresponded to codon-281 hotspot mutation found in human cancers including glioma (<http://www-p53.iarc.fr/>). In contrast, KO3 cells carried a silent mutation in codon 75 (Suppl. Fig. 3C). Interestingly, KO2 and KO3 cells displayed a marked down-regulation of p16^{INK4a} expression at both mRNA and protein levels (Suppl. Fig. 3D). p53 mutations were also found in KO4 and KO5 cell preparations (Suppl. Table 1). shNDUFA10 NPCs displayed a missense mutation in the p53 DNA binding domain (hotspot codon 135 in human p53; Suppl. Fig. 3E). In all cases, KO cell preparations and shNDUFA10 cells were analysed at passage 5-6 from isolation/infection (Suppl. Table 1). Notably, we were unable to detect p53 mutations/deletions in WT cells from four individual cell preparations up to passage 12-14 (Suppl. Table 1). Overall, our data suggest that inhibition of oxidative metabolism leads to p53 genetic inactivation in NPCs.

p53 mutational status, not p16^{INK4a} down-regulation, correlated with enhanced proliferative capacity, as KO1 and KO2 cells displayed a growth advantage over KO3 and WT cells (Fig. 3B and Suppl. Fig. 3D). KO3 cells grew even slower than WT cells (Fig. 3D). p53 loss-of-function mutations found in ETC-impaired cells correlated with increased ATP and lactate levels (Suppl. Fig. 3F), a phenotype observed in NPCs derived from the p53 germline KO (Fig. 3D-F) as well as in Cre-infected *p53^{flax/flax}* cells (Suppl. Fig. 4G, H). Furthermore, KO1 and KO2 cells displayed an impaired G1/S checkpoint upon IR, whereas KO3 cells behaved like wild-type cells (Suppl. Fig. 4). These data suggest that p53 loss is responsible for the growth and metabolic phenotypes observed

205
206
207
208
209
210
211
212
213
214
215
216
217
218
219
220
221
222
223
224
225
226
227
228
229
230
231
232
233
234
235
236
237
238
239
240
241
242
243
244
245
246
247
248
249
250
251
252
253
254
255
256
257
258
259
260
261
262
263
264
265
266
267
268
269
270
271
272

273
274
275
276
277
278
279
280
281
282
283
284
285
286
287
288
289
290
291
292
293
294
295
296
297
298
299
300
301
302
303
304
305
306
307
308
309
310
311
312
313
314
315
316
317
318
319
320
321
322
323
324
325
326
327
328
329
330
331
332
333
334
335
336
337
338
339
340

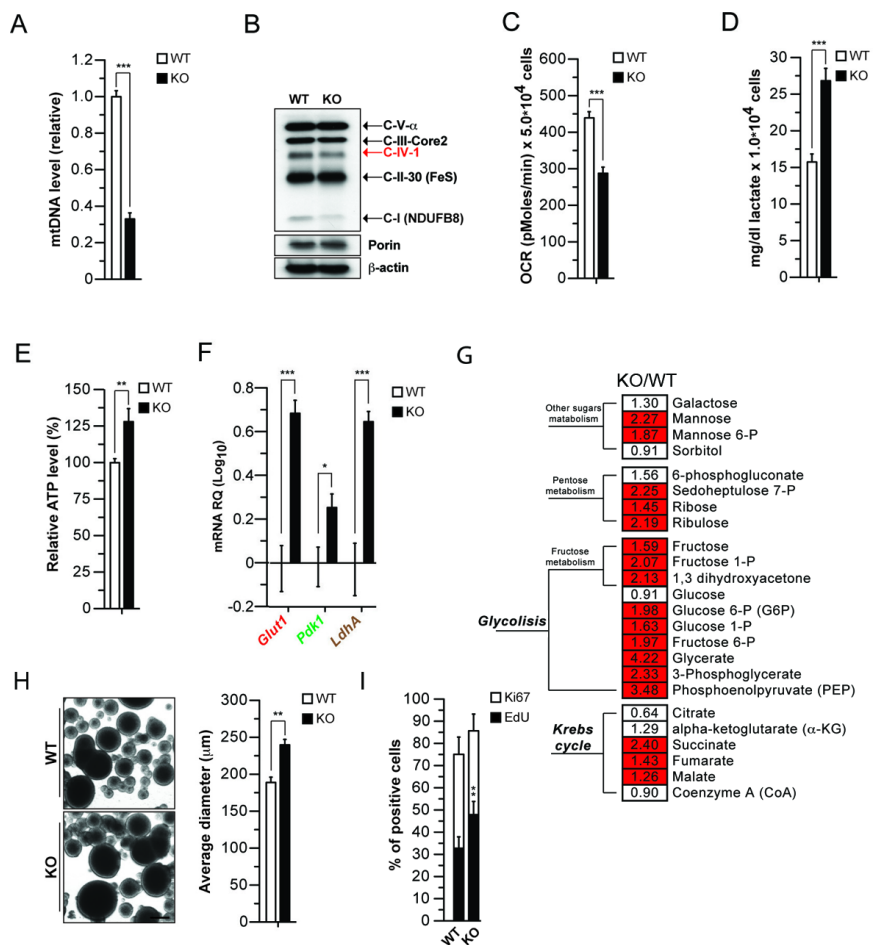


Fig. 2. Reduction in mitochondrial copy number leads to ETC defects, glycolysis induction and growth advantage(A) Relative quantification of mtDNA levels in wild type (WT) and TK2 KO (KO) NPCs using quantitative RT-PCR (QPCR; n=3, ***p<0.001); (B) Levels of ETC mtDNA-encoded (red) and nuclear-encoded (black) proteins at steady state using an antibody mix against OXPHOS complexes. Porin and β actin are shown as loading controls for mitochondria and total protein extracts respectively; (C) OCR in NPCs under basal conditions. Data are average of 3 independent experiments as mean \pm SEM. NPCs were obtained from n=3 animals for each genotype; ***p<0.001; Lactate (D) and relative ATP levels (E) in NPCs. Measurements were made in triplicate (Data are represented as mean \pm SEM for n=3; **p<0.01, ***p<0.001); (F) Expression of the genes *Glut1*, *Pdk1* and *LdhA* in WT and TK2 KO NPCs (expressed as levels over WT cells). (G) Heat-map showing the ratio of the metabolite levels between KO and WT NPCs, and their statistical significance of the difference (Welch's two samples t-test). Cells shaded in red indicate higher metabolite levels in KO NPCs with p<0.001. Cells not shaded indicate no significant difference (p>0.05). The number in each cell indicates fold changes over WT. (H) Proliferation of NPCs measured using the neurosphere assay. Neurosphere diameter is increased in re-stimulated KO NPCs (n=3 **p<0.001, Student's t-test). Scale bar corresponds to \approx 100 μ m. (I) Proliferation of NPCs by EdU labelling (2h) and immunodetection of Ki67. Graph shows quantification of EdU and Ki67.

upon ETC inhibition in NPCs. Indeed, when we reintroduced WT p53 in KO1 cells, we observed a rescue in *p21* expression and down-regulation of *Glut1*, *Glut3*, *LdhA* and *Pdk1* (Fig. 3C, D).

We next investigated the mechanisms underlying p53 loss upon inhibition of oxidative metabolism. As ETC dysfunction is known to promote alterations of cellular redox (28, 29) and ROS can directly cause DNA damage (30, 31), we hypothesized that ROS could be involved in causing p53 genetic inactivation in ETC-impaired NPCs. To test this, we analyzed KO cells at isolation from the SVZ. Indeed, we found that ROS are increased in KO cells (Fig. 3E), and this is associated with augmented 8-hydroxy-2'-deoxyguanosine levels, a marker of DNA oxidative damage (8-OHdG; Fig. 3F). 8-OHdG elevation correlated with increased γ H2AX foci and levels, suggesting induction of double strand breaks and ensuing DNA damage response activation (Fig. 3G). KO NPCs also displayed aberrant nuclear morphology with multi-lobated nuclei and increased number of micronuclei (Suppl. Fig. 5A). FACS analysis of KO cells also revealed increased hyper-diploid DNA content, an index of chromosomal abnormalities (Suppl. Fig. 5B). Similar changes in nuclear morphology were obtained when cells were cultured for 6 days in the presence of oligomycin (Suppl. Fig. 5C). To confirm the involvement of ROS in promotion of genomic instability, we treated WT and KO NPCs with the ROS scavenger NAC. Indeed, NAC normalized ROS levels, γ H2AX foci number and nuclear morphology (Suppl. Fig. 5D and Fig. 3H). Similarly, normalization of γ H2AX was achieved by culturing KO NPCs in low oxygen (Fig. 3I). Notably, freshly isolated KO cells displayed increased p53 activation, which was ROS-dependent and was associated with

reduced growth (Fig. 3J and Suppl. Fig. 5E). These findings suggest that increased selective pressure to overcome p53-mediated cell cycle arrest in the presence of mitogenic signals along with increased ROS-mediated DNA damage represents a potential mechanism for p53 loss in NPCs. To test this, we cultured KO cells in low and high O₂ from isolation and analyzed oxidative damage and the p53 status through passaging. While KO NPC preparations acquired p53 mutations in high O₂, we failed to detect any mutation in low O₂ conditions up to passage 8 (Suppl. Fig. 5F and Suppl. Table 1).

p53 inactivation is predicted to contribute to overcoming the growth suppressive response to oncogenic activation. Hence, we analysed the growth properties of WT and KO cells transduced with hRASV12 and control vector viral particles (Fig. 4A). hRASV12 KO cells displayed higher lactate and ATP levels (Fig. 4B). While oncogenic hRAS did not induce growth arrest in WT NPCs unlike in fibroblasts, hRASV12 KO cells grew faster in either the presence or absence of growth factors (Fig. 4C).

As p53 loss has been shown to promote HGG development in mouse via increased genomic instability (21), we reasoned that ETC-impaired, p53-deficient cells could become tumorigenic. To this end, we orthotopically transplanted WT and KO (KO1) cells into the brain of recipient mice. To allow for identification of transplanted cells, NPCs were first transduced with IRES-GFP retroviral particles. None of the mice injected with WT cells developed brain tumors (0/13). In contrast, KO IRES-GFP cells were able to form poorly differentiated tumors in transplanted immune-compromised (1/4) as well as immune-competent (1/5) mice, which diffusely infiltrated the host brain (Fig. 4D, Suppl.

341
342
343
344
345
346
347
348
349
350
351
352
353
354
355
356
357
358
359
360
361
362
363
364
365
366
367
368
369
370
371
372
373
374
375
376
377
378
379
380
381
382
383
384
385
386
387
388
389
390
391
392
393
394
395
396
397
398
399
400
401
402
403
404
405
406
407
408

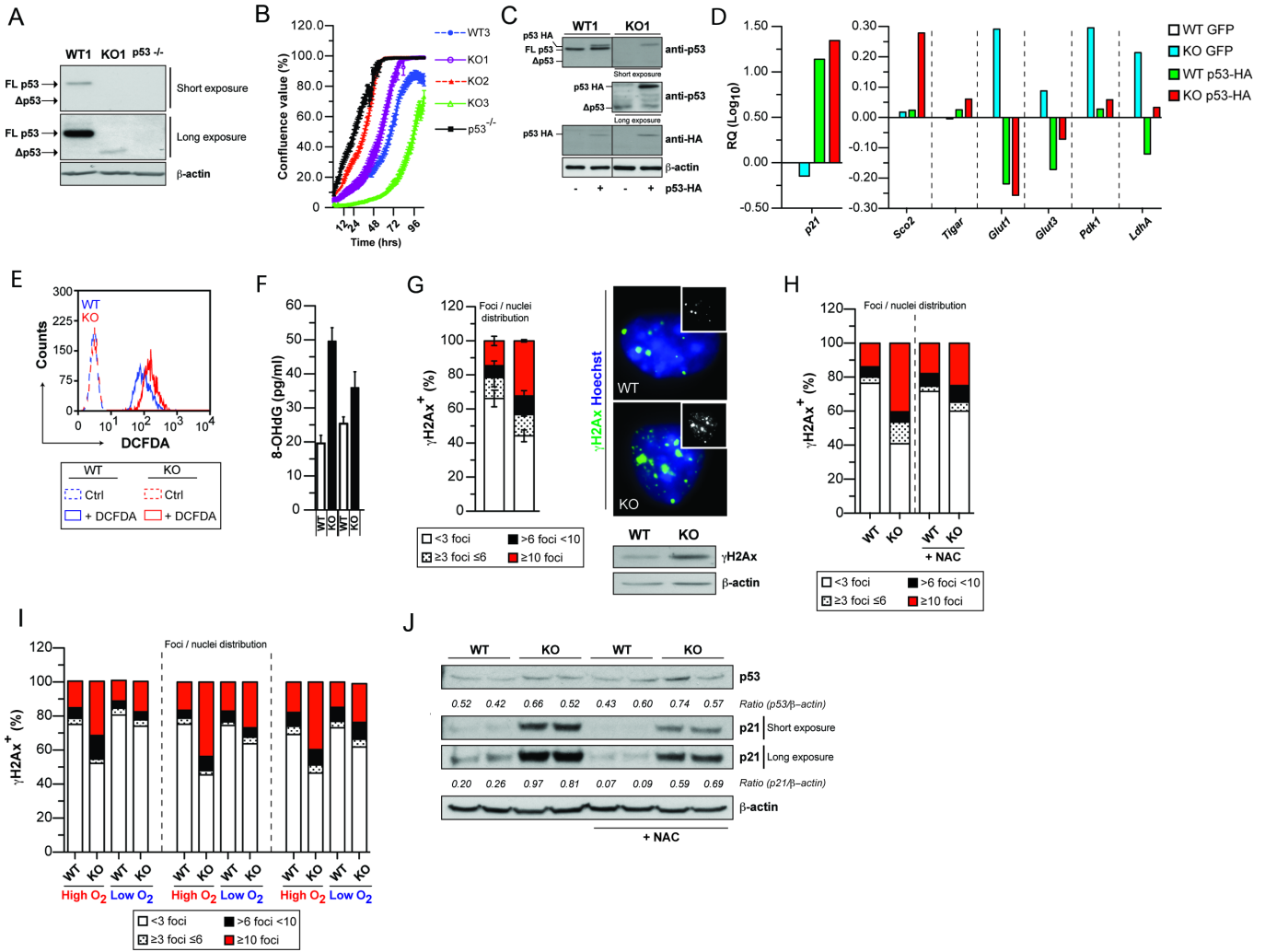


Fig. 3. ETC impairment leads to p53 genetic inactivation (A) Western blot showing expression of full length (FL) p53 as well as the delete Δ p53 form in WT and TK2 KO (KO) NPCs. $p53^{-/-}$ NPCs were used as negative control. (B) Increased growth properties of KO1, KO2 and p53 KO NPCs as assessed by a High Definition (HD) imaging system; growth curves representative of 2 independent experiments; (C) Western blot analysis of WT (WT1) and KO (KO1) NPCs infected with WT-p53-HA GFP or GFP alone (left panel). (D) Representative expression analysis of $p21^{WAF1}$, *Sco2*, *Tigar*, *Glut1*, *Glut3*, *Pdk1*, and *Ldha* levels (right panel) upon retroviral expression of exogenous WT-p53. Results are normalized to β -actin expression level. (E) Representative plot of intracellular ROS levels, as assessed by FACS analysis using the DCFDA dye; (F) Quantification of oxidized DNA marker 8-hydroxy-2'-deoxyguanosine (8-OHdG) in WT and KO NPCs cultured in normoxic condition; (G) Percentage of cells displaying defined number of γ H2Ax foci/nuclei (left panel). Immunofluorescence analysis of phosphorylated histone γ H2Ax foci (top right panel) in NPCs. Western blot analysis of γ H2Ax levels (bottom right panel). (H) γ H2Ax foci quantification in WT and TK2 KO NPCs with or without the antioxidant N-acetyl cysteine (NAC; 0.1 mM); (I) γ H2Ax in three independent preparations (see Table S2) of KO and matched WT NPCs in high and low O_2 . The graph (left) shows the percentage of cells displaying defined number of γ H2Ax foci / nuclei. (J) Western blot analysis of p53 and $p21^{WAF1}$ (p21) levels at steady state in the presence or absence of NAC. Cells were treated for 7days with NAC before any measurement.

Table 2). Overall, these findings indicate that impairment of mitochondrial respiration in neural stem cells can result in inactivation of the p53 pathway and tumor transformation.

Finally, we investigated whether respiratory chain alterations correlated with p53 mutations in primary high-grade glioma (HGG) cells. To this end, we took advantage of a panel of glioma-initiating neural stem (GNS) cells derived from resected HGG (G1, G2, G3, G4, G144, G166). These cells represent a subpopulation within the bulk of established tumors bearing neural stem-like features, which can initiate glioma when transplanted in recipient animals (32). We noticed that a number of lines displayed enhanced growth properties (G3, G4, G144 and G166; Suppl. Fig. 6A). Among them, only G3, G144 and G166 also showed elevated lactate levels and extracellular acidification rate (ECAR; Suppl. Fig. 6B). These cells carried hotspot mutations in the p53 DNA binding domain (Suppl. Fig. 6C-D). We then explored the status of the respiratory chain by using the MitoProfile®

Total OXPHOS antibody cocktail and individual antibodies for different ETC components (Suppl. Fig. 6E). Interestingly, p53-mutated cells showed reduced expression of the mtDNA-encoded C-IV subunit I (C-IV-1) and C-IV-2, as well as the nuclear DNA-encoded C-IV-4 (Suppl. Fig. 6E). We then measured whether these changes correlated with impaired OCR. Uncoupling the mitochondria with an optimal concentration of FCCP (3 μ M) rapidly increased respiration yielding an OCR value for maximal O_2 consumption in p53-proficient cells, while it was significantly lower in p53-mutated GNS cells (Suppl. Fig. 6F,G). Consistent with the decreased expression of C-IV components, we observed significant impairment of C-IV activity (Suppl. Fig. 6H) using treatment with antimycin A, which blocks electron flux to complex III, and a complex IV direct agonist (N,N,N',N'-tetramethyl-p-phenylenediamine (TMPD)/ ascorbate). Changes in ETC subunit levels were not recapitulated by p53 loss alone or concomitant with expression of p53 mutants in NPCs, suggesting that alter-

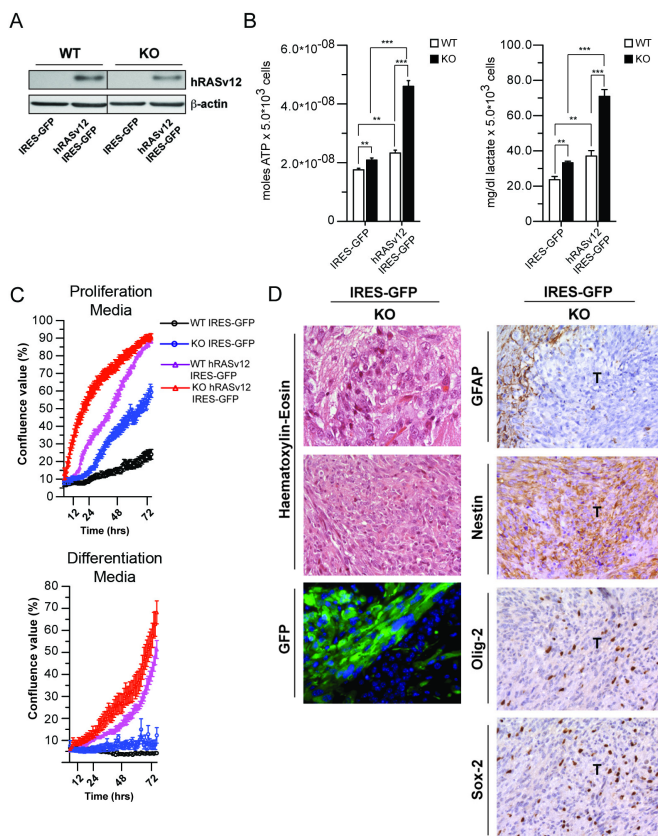


Fig. 4. ETC-impaired cells are susceptible to neoplastic transformation (A) Western blot analysis of WT and KO (KO1 preparation) NPCs infected with hRASv12 IRES-GFP or IRES-GFP alone. (B) ATP and lactate production under basal conditions in WT and KO NPCs transduced with either IRES-GFP or hRASv12 IRES-GFP retrovirus. (** p < 0.01, *** p < 0.0001, Student's t-test, error bars are s.d.) (C) Growth curves analysis and representative images of WT and KO cells transduced with control (IRES-GFP) or hRASv12 IRES-GFP retroviral particles in proliferation (left) and differentiation (right) culture conditions. (D) Left panel: histological and fluorescence microscopy analysis of allografts, derived from KO IRES-GFP cells. WT and KO cells were cultured as neurospheres, transduced with IRES-GFP and orthotopically allografted into the caudoputamen of NOD/SCID immunosuppressed mice. No tumours were obtained in mice in which WT cells were xenografted. H&E histology shows large, cytoplasm rich cells in KO tumour cells. Anti-GFP immunostaining was used to identify the tumour-initiating cells (bottom row). Right panel: immunohistochemical staining for the astrocyte marker GFAP shows that all tumours are negative with positive cells only in the adjacent host tissue. Immunohistochemical analysis of the neural stem cell marker Nestin shows a strong, diffuse labeling of tumor cells. The neural progenitor marker Olig-2 shows that many but not all of tumor cells present strong nuclear expression. The progenitor cell marker Sox-2 is expressed in a smaller subset of tumor cells. Scale bar corresponds to 80 μ m (first row), 320 μ m (second row), and 160 μ m (remaining panels);

ations in ETC subunit composition may not be downstream to p53 inactivation (Suppl. Fig. 6I, J) Altogether, these findings indicate that ETC alterations are associated with p53 mutations and glycolytic metabolism in GNS cells.

Discussion

This work suggests a role for mitochondrial metabolism in the regulation of tumor suppressive mechanisms and transformation in the central nervous system (CNS). In particular, we showed that respiratory chain dysfunction can lead to p53 genetic inactivation and transformation in NPCs (Suppl. Fig. 7). Furthermore, in accordance with the reported role of p53 in suppressing transformation of NPCs (18-22), ETC-impaired/p53-deficient NPCs

grow faster upon oncogenic activation and are capable of forming brain tumors in a subset of orthotopically-transplanted animals. The incomplete penetrance observed in these experiments may be due to the fact that other cooperative oncogenic events may have to be acquired, as previously suggested (21) and indeed these might be favored by ROS increase as well as by p53 loss. Genome stability could also be affected via metabolic stress-dependent inhibition of metabolism-sensitive DNA repair enzymes, such as PARP (33), or indirectly via iron/sulphur (Fe/S) cluster formation (34-37) as part of a mitochondrial retrograde signaling.

Our data indicate that selective pressure to overcome ROS-mediated p53 activation along with increased ROS-mediated DNA damage contribute to p53 genetic loss in NPCs. Loss of p53 in turn leads to a metabolic switch and potentially favors acquisition of other oncogenic mutations to be yet identified. The importance of the redox state in the mechanism leading to p53 mutation is clearly shown by the fact that by reducing oxygen levels we were able to block the appearance of p53 mutations in ETC-impaired NPCs. It is conceivable that ROS originating from dysfunctional mitochondria synergize with ROS produced by growth factor signaling, as NPCs are cultured in the presence of highly mitogenic growth factors. *In vivo*, elevated ROS levels within the highly vascular SVZ niche have been proposed to fuel NPC expansion via growth factor signaling (38, 39). However, ROS can also lead to respiratory chain dysfunction via ROS-mediated damage to ETC components and mitochondrial DNA (mtDNA) (30, 40-42). Respiratory chain inhibition would further augment ROS generation, thus promoting a vicious circle of oxidative stress (28, 29, 43). Finally, we observed an association between altered ETC composition, dysfunctional respiratory chain function and p53 mutations in primary HGG cells. These findings suggest a novel twist in the relationship between oxidative metabolism, the p53 tumor suppressive pathway and cellular redox status in somatic stem cells (Suppl. Fig. 7): while in normal cells p53 positively regulates oxidative metabolism and anti-oxidant defenses, inhibition of the respiratory chain can lead to p53 genetic inactivation via a ROS-dependent mechanism, eventually contributing to malignant transformation.

Based on the classical model of tumorigenesis, an initial mutation of an oncogene or a tumor suppressor leads to subsequent molecular changes ultimately resulting in malignant transformation, including alterations of mitochondrial metabolism. We propose an additional model, whereby an initial alteration of oxidative metabolism can lead to increased mutation rate that eventually results in oncogenic mutations and tumor transformation. In highly proliferative epithelial tissues, which are more exposed to environmental factors, the first model would apply more frequently. In this respect, UV irradiation has recently been demonstrated to induce accumulation of p53 mutations at high frequency, thus accelerating BRAF(V600E)-driven melanomagenesis (44). In contrast, in progenitor/stem cells within the adult brain, which are less exposed to environmental insults, the initial event might be a metabolic defect, such as alterations of mitochondrial respiration. In fact, with the exception of exposure to ionizing radiations a strong correlation between brain tumors and exposure to environmental carcinogens was never clearly demonstrated (45, 46). It is important to note that there is lack of evidence that hereditary diseases carrying mutations in nuclear DNA and mtDNA-encoded mitochondrial factors, such as TK2, display increased cancer susceptibility. However, the severity of phenotypes affecting cells in these conditions may not provide an incontrovertible answer to this question. In particular, neurodegeneration phenotypes observed in these hereditary diseases could have an earlier onset compared to more indolent tumor phenotypes, thus limiting the value of an epidemiological approach.

Experimental procedures

681
682
683
684
685
686
687
688
689
690
691
692
693
694
695
696
697
698
699
700
701
702
703
704
705
706
707
708
709
710
711
712
713
714
715
716
717
718
719
720
721
722
723
724
725
726
727
728
729
730
731
732
733
734
735
736
737
738
739
740
741
742
743
744
745
746
747
748

Animals

Germline TK2 knockout (KO) mice that harbor a progressive loss of mtDNA, were developed by Xiaoshan Z. and colleagues in A. Karlsson's laboratory (Karolinska Institute, Stockholm, Sweden) (26).

Mouse neural stem cell culture

Isolation of adult mouse NPCs was performed as previously described. Brains were dissected to remove the olfactory bulbs, cerebellum and brainstem. An area encompassing the SVZ surrounding the lateral wall of the forebrain ventricle was dissected. Tissue was dissociated with accutase for 15mins at 37C and mechanically dissociated. Cells were plated onto laminin pre-coated culture dish in expansion media (RHA-B media supplemented with 10 ng/mL of both bFGF and EGF. For neurosphere cultures, cells were plated at clonal density (20×10^3 cells ml^{-1} and cultured for 7 days in vitro (DIV). For differentiation analysis, single cells were plated at 2.5×10^5 cells ml^{-1} on laminin-coated glass coverslips ($\varnothing 13$ mm) in expansion media, before the subsequent withdrawal of bFGF and EGF growth factors to facilitate differentiation over 8 DIV (3 days without EGF followed by 8 days in the absence of growth factors).

ATP levels and lactate production

Total ATP levels were determined using the CellTiter-Glo[®] Luminescent assay as per the manufacture's instruction (Promega). Lactate was measured using the Trinity Biotech lactate assay. Data are expressed as mole of ATP/relative ATP level (%) and mg/dl lactate respectively and all the values were normalized to cells number.

Metabolic profiling

Metabolic profiles were obtained for each individual genotype using the Metabolon Platform (Metabolon Inc. NC, USA), as described in (47). Each sample consisted of 6 Sample preparation (5 for WT cells) was conducted

1. Frezza C & Gottlieb E (2009) Mitochondria in cancer: not just innocent bystanders. *Semin Cancer Biol* 19(1):4-11.
2. Amary MF, et al. (2011) IDH1 and IDH2 mutations are frequent events in central chondrosarcoma and central and periosteal chondromas but not in other mesenchymal tumours. *J Pathol* 224(3):334-343.
3. Prensner JR & Chinnaiyan AM (2011) Metabolism unhinged: IDH mutations in cancer. *Nat Med* 17(3):291-293.
4. Reitman ZJ, et al. (2011) Profiling the effects of isocitrate dehydrogenase 1 and 2 mutations on the cellular metabolome. *Proc Natl Acad Sci U S A* 108(8):3270-3275.
5. Cairns RA & Mak TW (2013) Oncogenic isocitrate dehydrogenase mutations: mechanisms, models, and clinical opportunities. *Cancer discovery* 3(7):730-741.
6. DeHaan C, et al. (2004) Mutation in mitochondrial complex I ND6 subunit is associated with defective response to hypoxia in human glioma cells. *Mol Cancer* 3:19.
7. Kirches E, et al. (2001) High frequency of mitochondrial DNA mutations in glioblastoma multiforme identified by direct sequence comparison to blood samples. *Int J Cancer* 93(4):534-538.
8. Larman TC, et al. (2012) Spectrum of somatic mitochondrial mutations in five cancers. *Proc Natl Acad Sci U S A* 109(35):14087-14091.
9. Lueth M, et al. (2009) Somatic mitochondrial mutations in pilocytic astrocytoma. *Cancer Genet Cytogenet* 192(1):30-35.
10. Marin-Valencia I, et al. (2012) Analysis of tumor metabolism reveals mitochondrial glucose oxidation in genetically diverse human glioblastomas in the mouse brain in vivo. *Cell Metab* 15(6):827-837.
11. Oliva CR, et al. (2010) Acquisition of temozolomide chemoresistance in gliomas leads to remodeling of mitochondrial electron transport chain. *J Biol Chem* 285(51):39759-39767.
12. Vega A, et al. (2004) mtDNA mutations in tumors of the central nervous system reflect the neutral evolution of mtDNA in populations. *Oncogene* 23(6):1314-1320.
13. Kiebish MA, Han X, Cheng H, & Seyfried TN (2009) In vitro growth environment produces lipidomic and electron transport chain abnormalities in mitochondria from non-tumorigenic astrocytes and brain tumours. *ASN Neuro* 1(3).
14. Zhou Y, et al. (2011) Metabolic alterations in highly tumorigenic glioblastoma cells: preference for hypoxia and high dependency on glycolysis. *J Biol Chem* 286(37):32843-32853.
15. Jones RG & Thompson CB (2009) Tumor suppressors and cell metabolism: a recipe for cancer growth. *Genes Dev* 23(5):537-548.
16. Lane D & Levine A (2010) p53 Research: the past thirty years and the next thirty years. *Cold Spring Harb Perspect Biol* 2(12):a000893.
17. Muller PA & Vousden KH (2013) p53 mutations in cancer. *Nature cell biology* 15(1):2-8.
18. Alicantara Llaguno S, et al. (2009) Malignant astrocytomas originate from neural stem/progenitor cells in a somatic tumor suppressor mouse model. *Cancer Cell* 15(1):45-56.
19. Chow LM, et al. (2011) Cooperativity within and among Pten, p53, and Rb pathways induces high-grade astrocytoma in adult brain. *Cancer Cell* 19(3):305-316.
20. Jacques TS, et al. (2010) Combinations of genetic mutations in the adult neural stem cell compartment determine brain tumour phenotypes. *EMBO J* 29(1):222-235.
21. Wang Y, et al. (2009) Expression of mutant p53 proteins implicates a lineage relationship between neural stem cells and malignant astrocytic glioma in a murine model. *Cancer Cell* 15(6):514-526.
22. Zheng H, et al. (2008) p53 and Pten control neural and glioma stem/progenitor cell renewal and differentiation. *Nature* 455(7216):1129-1133.
23. Llaguno SA, Chen J, Kwon CH, & Parada LF (2008) Neural and cancer stem cells in tumor suppressor mouse models of malignant astrocytoma. *Cold Spring Harbor symposia on quantitative biology* 73:421-426.
24. Akman HO, et al. (2008) Thymidine kinase 2 (H126N) knockin mice show the essential role of balanced deoxynucleotide pools for mitochondrial DNA maintenance. *Hum Mol Genet* 17(16):2433-2440.

using a proprietary series of organic and aqueous extractions to remove the protein fraction while allowing maximum recovery of small molecules. The resulting extract was divided into two fractions; one for analysis by LC and one for analysis by GC. Samples were placed briefly on a TurboVap[®] (Zymark) to remove the organic solvent. Samples were then frozen, vacuum dried and then prepared for either LC/MS or GC/MS. Compounds above the detection threshold were identified by comparison to library entries of purified standards or recurrent unknown entities. Identification of known chemical entities was based on comparison to metabolomic library entries of purified standards.

Acknowledgements.

We thank Salvador Moncada (UCL, UK), Doug Turnbull, Robert Taylor (University of Newcastle, UK), Andrea Cossarizza (University of Modena and Reggio Emilia, Italy), Doug Green (St Jude Childrens Hospital, Memphis, USA), Sarah Ann-Martin (Barts Cancer Institute, London, UK), Steven Pollard (Edinburgh University), Pablo Rodriguez-Viciana and Asim Khwaja (UCL, UK) for reagents, support and critical discussion. Finally, we thank the UCL Scientific Services, the CAGE facility and the UCL Biological Services Unit. In PS lab, this work was supported by Medical Research Council, The Brain Tumour Charity (through a generous donation from the Brian Cross family) and by a donation from David Hunter and Wendy Tansey in memory of Peter Clark. SB and NH received support from UCLH CBRC and the Brain Tumour Charity. SB (IoN) acknowledges the Neurosurgical team at the National Hospital for their continued support of the brain tumor bank. VG was recipient of travel fellowships from Boehringer Ingelheim (2010) and EMBO (2011). This work was also in part supported by AIRC IG 11450 and Ministero Sanità Ricerca Finalizzata (2009) to VDL.

25. Bartesaghi S, et al. (2010) Loss of thymidine kinase 2 alters neuronal bioenergetics and leads to neurodegeneration. *Hum Mol Genet* 19(9):1669-1677.
26. Zhou X, et al. (2008) Progressive loss of mitochondrial DNA in thymidine kinase 2-deficient mice. *Hum Mol Genet* 17(15):2329-2335.
27. Kim EL, et al. (2005) Comparative assessment of the functional p53 status in glioma cells. *Anticancer research* 25(1A):213-224.
28. Li N, et al. (2003) Mitochondrial complex I inhibitor rotenone induces apoptosis through enhancing mitochondrial reactive oxygen species production. *J Biol Chem* 278(10):8516-8525.
29. Muller FL, Liu Y, & Van Remmen H (2004) Complex III releases superoxide to both sides of the inner mitochondrial membrane. *J Biol Chem* 279(47):49064-49073.
30. Ziech D, Franco R, Pappa A, & Panayiotidis MI (2011) Reactive oxygen species (ROS)-induced genetic and epigenetic alterations in human carcinogenesis. *Mutation research* 711(1-2):167-173.
31. Sedelnikova OA, et al. (2010) Role of oxidatively induced DNA lesions in human pathogenesis. *Mutation research* 704(1-3):152-159.
32. Pollard SM, et al. (2009) Glioma stem cell lines expanded in adherent culture have tumor-specific phenotypes and are suitable for chemical and genetic screens. *Cell Stem Cell* 4(6):568-580.
33. Luo X & Kraus WL (2012) On PAR with PARP: cellular stress signaling through poly(ADP-ribose) and PARP-1. *Genes Dev* 26(5):417-432.
34. Stehling O, Elsasser HP, Bruckel B, Muhlenhoff U, & Lill R (2004) Iron-sulfur protein maturation in human cells: evidence for a function of frataxin. *Hum Mol Genet* 13(23):3007-3015.
35. Thierbach R, et al. (2012) Specific alterations of carbohydrate metabolism are associated with hepatocarcinogenesis in mitochondrially impaired mice. *Hum Mol Genet* 21(3):656-663.
36. Thierbach R, et al. (2005) Targeted disruption of hepatic frataxin expression causes impaired mitochondrial function, decreased life span and tumor growth in mice. *Hum Mol Genet* 14(24):3857-3864.
37. Veatch JR, McMurray MA, Nelson ZW, & Gottschling DE (2009) Mitochondrial dysfunction leads to nuclear genome instability via an iron-sulfur cluster defect. *Cell* 137(7):1247-1258.
38. Le Belle JE, et al. (2011) Proliferative neural stem cells have high endogenous ROS levels that regulate self-renewal and neurogenesis in a PI3K/Akt-dependant manner. *Cell Stem Cell* 8(1):59-71.
39. Ottone C, et al. (2014) Direct cell-cell contact with the vascular niche maintains quiescent neural stem cells. *Nature cell biology* 16(11):1045-1056.
40. Kowaltowski AJ & Vercesi AE (1999) Mitochondrial damage induced by conditions of oxidative stress. *Free Radic Biol Med* 26(3-4):463-471.
41. Moncada S & Erusalimsky JD (2002) Does nitric oxide modulate mitochondrial energy generation and apoptosis? *Nat Rev Mol Cell Biol* 3(3):214-220.
42. Choksi KB, Boylston WH, Rabek JP, Widger WR, & Papaconstantinou J (2004) Oxidatively damaged proteins of heart mitochondrial electron transport complexes. *Biochim Biophys Acta* 1688(2):95-101.
43. Wallace DC (2005) A mitochondrial paradigm of metabolic and degenerative diseases, aging, and cancer: a dawn for evolutionary medicine. *Annu Rev Genet* 39:359-407.
44. Viros A, et al. (2014) Ultraviolet radiation accelerates BRAF-driven melanomagenesis by targeting TP53. *Nature* 511(7510):478-482.
45. Schwartzbaum JA, Fisher JL, Aldape KD, & Wrensch M (2006) Epidemiology and molecular pathology of glioma. *Nature clinical practice. Neurology* 2(9):494-503; quiz 491 p following 516.
46. Ostrom QT, et al. (2014) The epidemiology of glioma in adults: a "state of the science" review. *Neuro-oncology*.
47. Tufi R, et al. (2014) Enhancing nucleotide metabolism protects against mitochondrial dysfunction and neurodegeneration in a PINK1 model of Parkinson's disease. *Nature cell biology* 16(2):157-166.

Please review all the figures in this paginated PDF and check if the figure size is appropriate to allow reading of the text in the figure.

If readability needs to be improved then resize the figure again in 'Figure sizing' interface of Article Sizing Tool.